Electronic Supplementary Information

for

New Class of Artificial Enzyme Composed of Mn-Porphyrin, Imidazole and Cucurbit[10]uril Toward Therapeutic Antioxidant

Riku Kubota*[a], Taiga Takabe[a], Kohe Arima[a], Hideaki Taniguchi,[a] Shoichiro Asayama[a] and Hiroyoshi Kawakami*[a]

*E-mail: r-kubota@tmu.ac.jp

kawakami-hiroyoshi@tmu.ac.jp

[a]*Department of Applied Chemistry, Tokyo Metropolitan University, Minami-osawa 1-1, Hachioji, Tokyo 192-0397, Japan.*

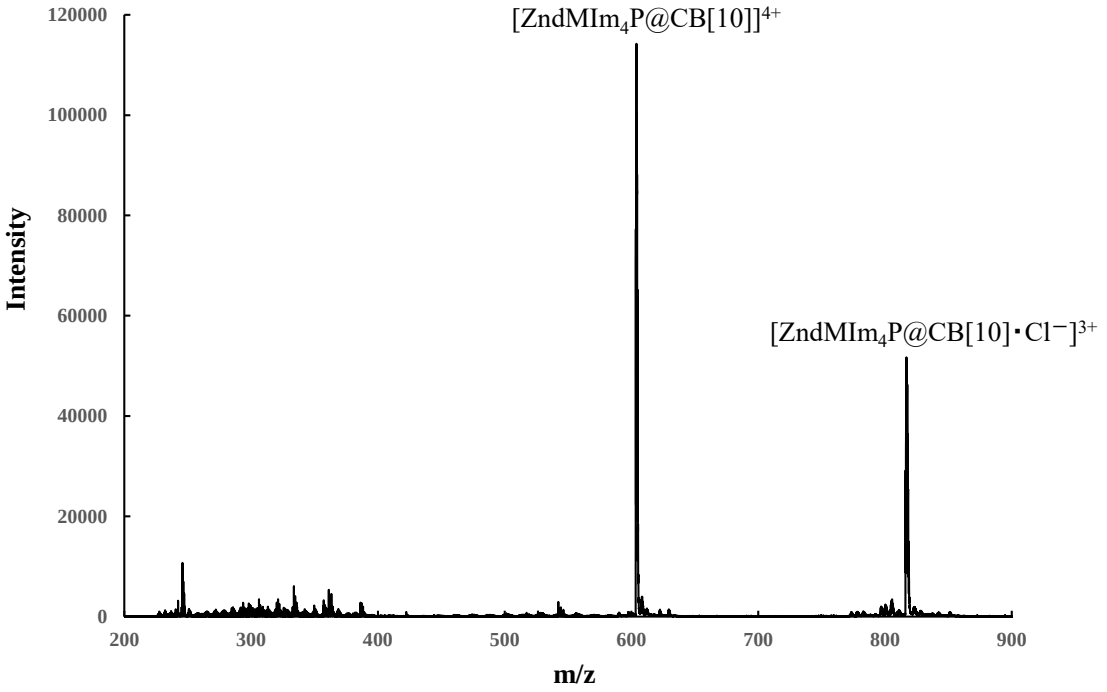

Fig. S1 ESI-MS spectrum of ZndMIm$_4$P@CB[10].
[ZndMIm$_4$P@CB[10]]$^{4+}$; Anal: 603.92. Found: 603.98.
[ZndMIm$_4$P@CB[10] · Cl$^-$]$^{3+}$; Anal: 816.91. Found: 816.97.

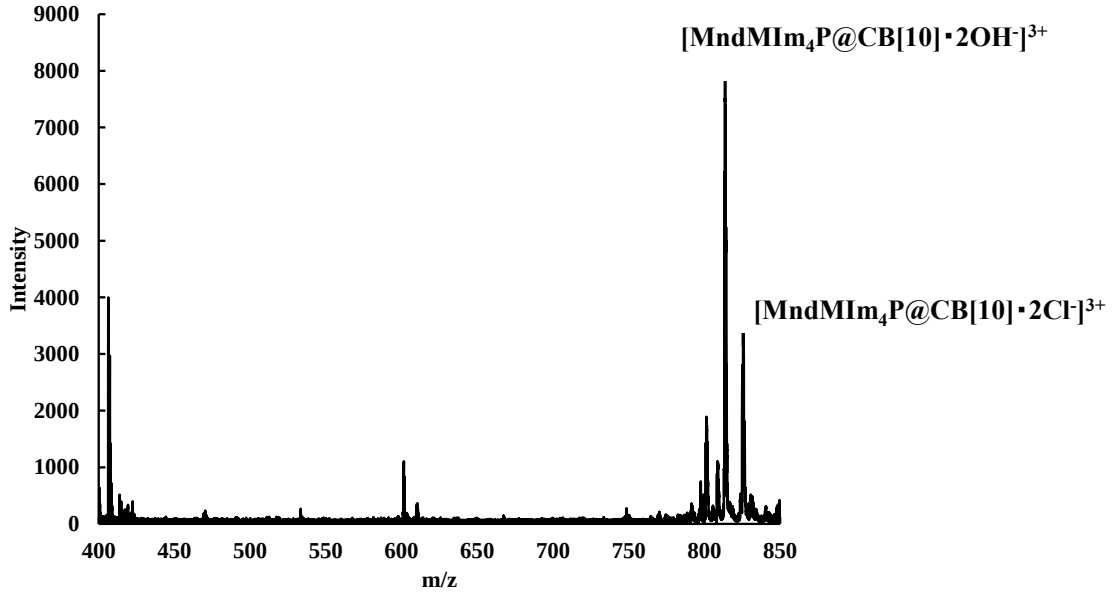

Fig. S2 ESI-MS spectrum of MndMIm$_4$P@CB[10].
[MndMIm$_4$P@CB[10] · 2OH$^-$]$^{3+}$; Anal: 813.26. Found: 813.32.
[MndMIm$_4$P@CB[10] · 2Cl$^-$]$^{3+}$; Anal: 825.57. Found: 825.64.

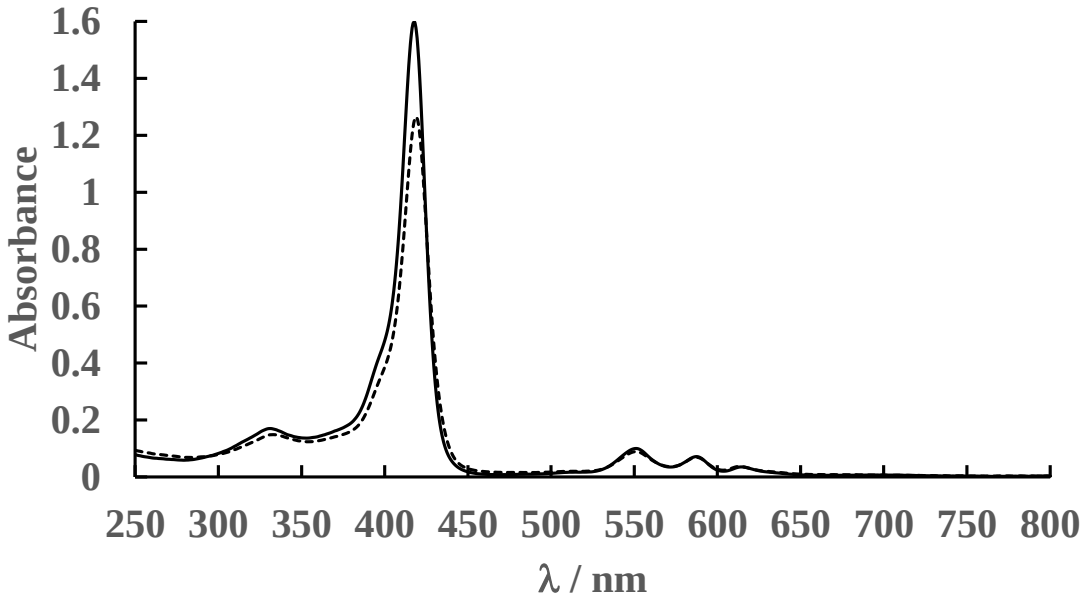

Fig. S3 UV/vis spectrum of 17.8 μM ZndMIm$_4$P alone (solid line) and 17.8 μM ZndMIm$_4$P@CB[10] (dotted line) in pure water.

ZndMIm$_4$P λ_{max}: 418 nm, 551 nm, 587 nm.

ZndMIm$_4$P@CB[10] λ_{max}: 419 nm, 551 nm, 587 nm.

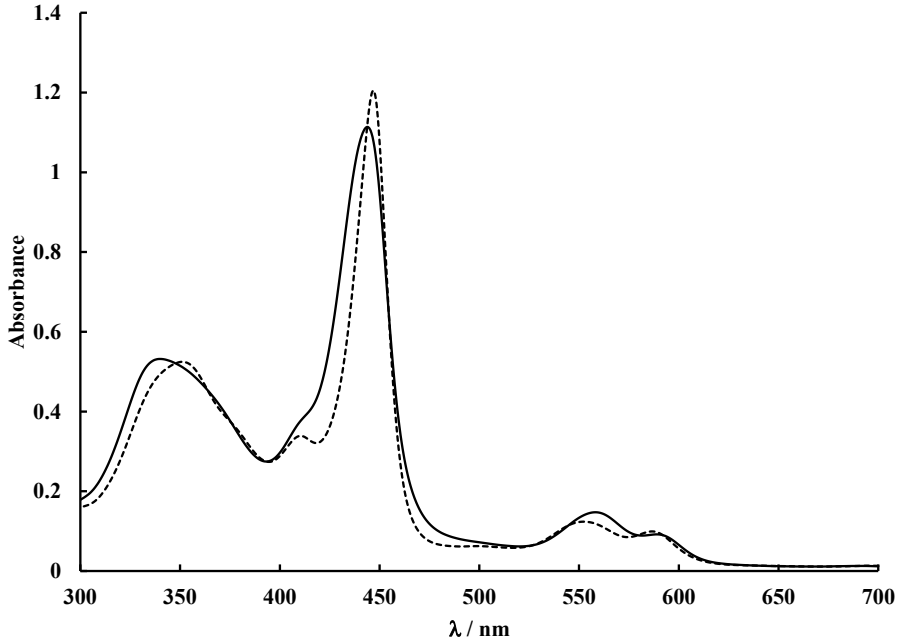

Fig. S4 UV/vis spectrum of 9.0 μM MndMIm$_4$P (solid line) and 9.0 μM MndMIm$_4$P@CB[10] (dotted line) in 25 mM phosphate buffer (pH 7.4).

MndMIm$_4$P λ_{max}: 443.5 nm, 558.5 nm, 589.5 nm.

MndMIm$_4$P@CB[10] λ_{max}: 447 nm, 553 nm, 586.5 nm.

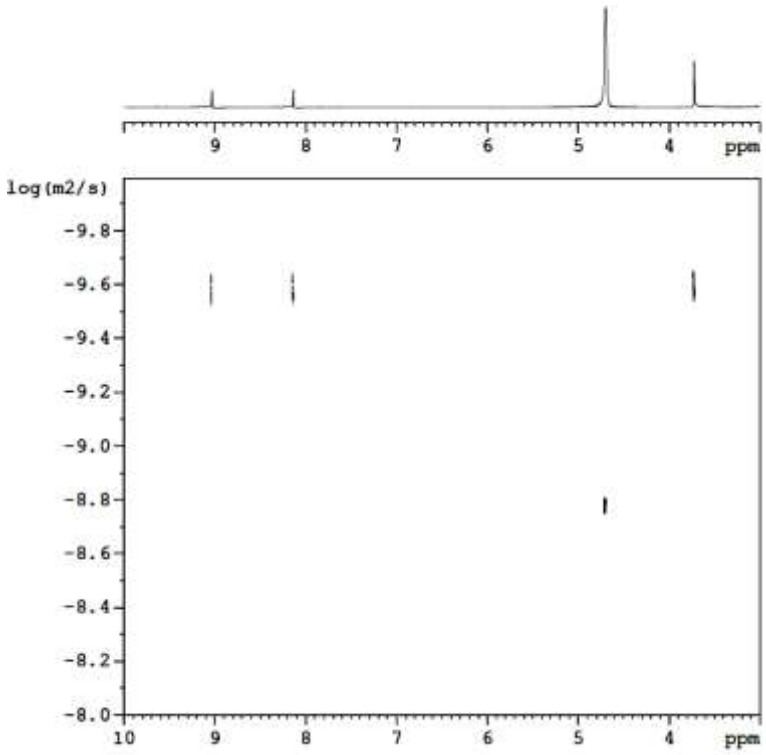

Fig. S5 DOSY spectrum of ZndMIm$_4$P alone (25℃, 500 MHz, D_2O).

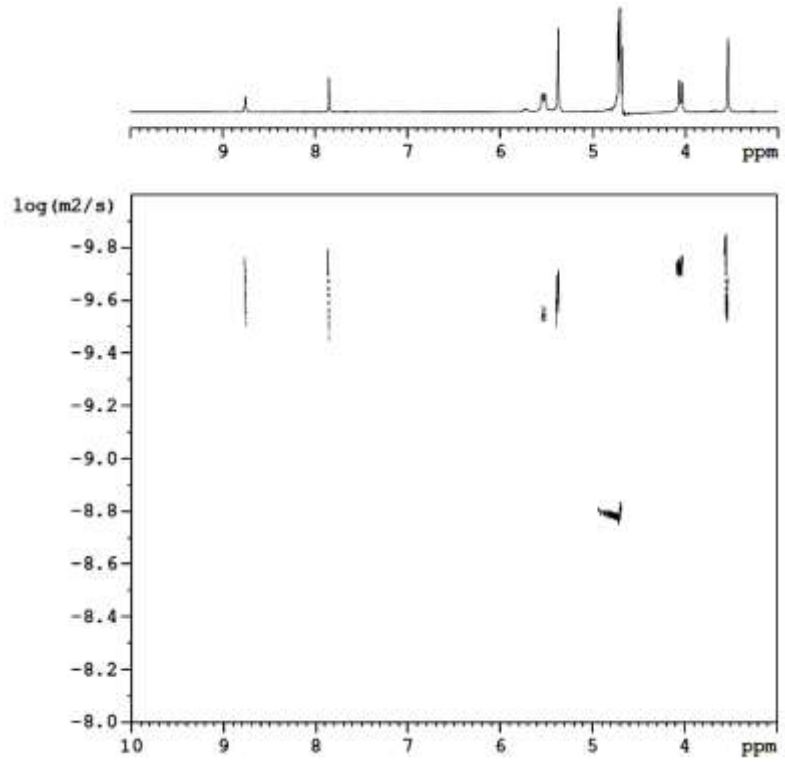

Fig. S6 DOSY spectrum of ZndMIm$_4$P@CB[10] (25℃, 500 MHz, D_2O).

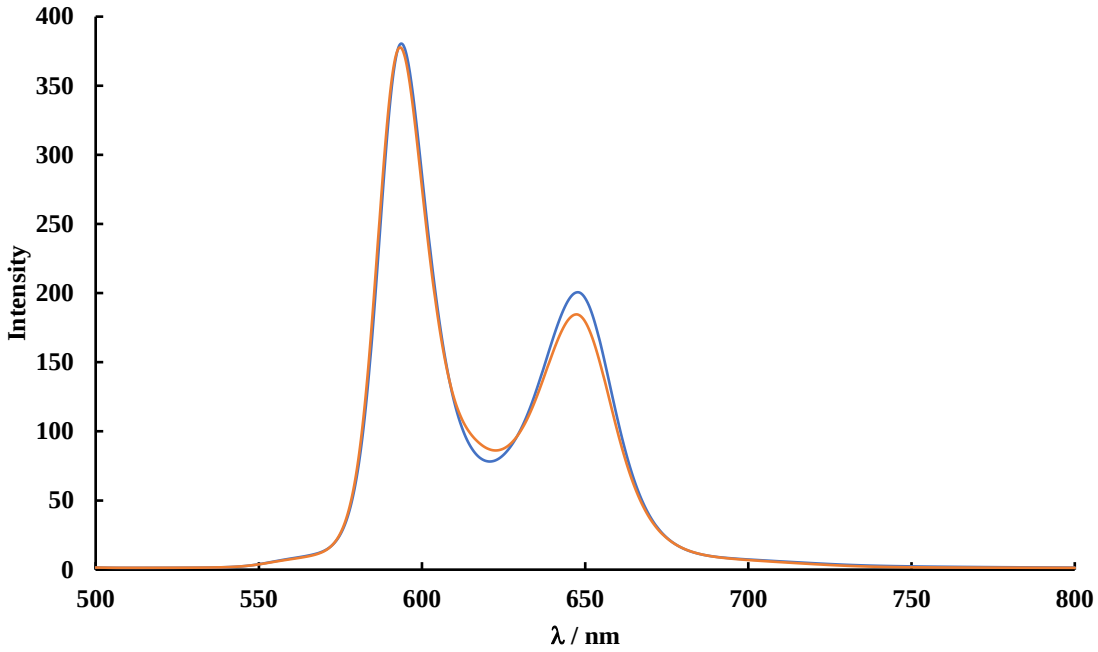

Fig. S7 Fluorescent spectrum of ZndMIm$_4$P (blue) and ZndMIm$_4$P@CB[10] (orange) in pure water measured at the same concentration per ZndMIm$_4$P (7.5 μM). ZndMIm$_4$P and ZndMIm$_4$P@CB[10] were excited at 423.5 nm where absorbance of ZndMIm$_4$P and ZndMIm$_4$P@CB[10] are identical.

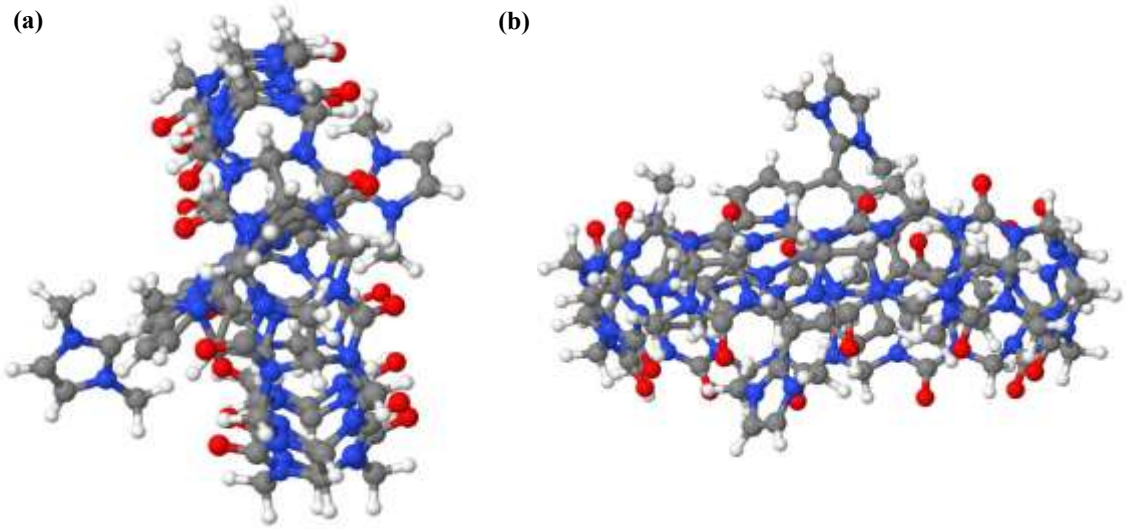

Fig. S8 DFT-minimized geometry of ZndMIm$_4$P@CB[10] (B3LYP/6-31G*). (a) side view, (b) top view.

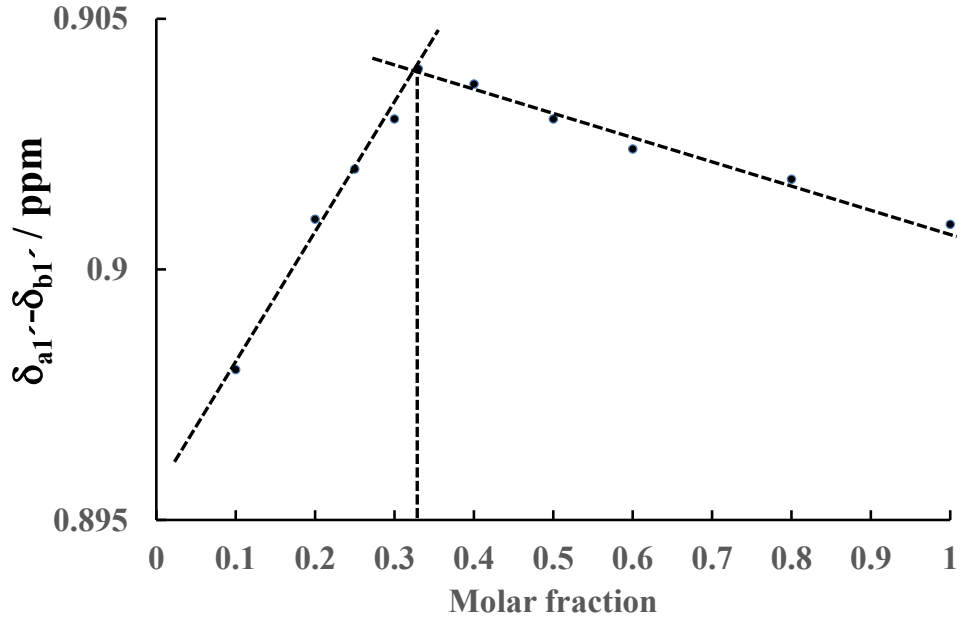

Fig. S9 Job`s plot for mixtures of ZndMIm$_4$P@CB[10] and imidazole at a total concentration of 0.5 mM.

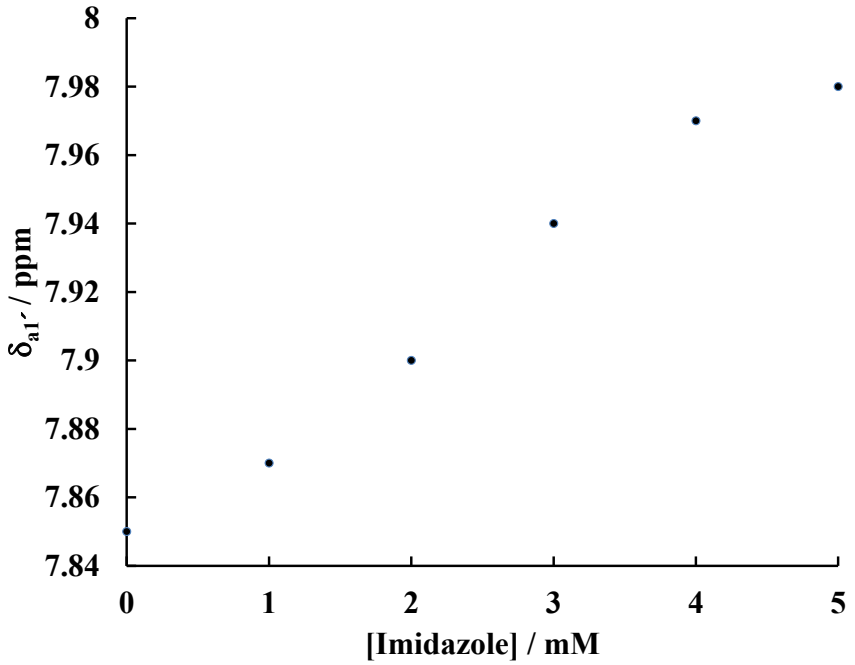

Fig. S10 Plot of the chemical shift (a_1´ of 1.0 mM ZndMIm$_4$P@CB[10]) as a function of imidazole concentration. The curve fitting analysis using TitrationFit program to determine $K_{a2} = 6.8 \times 10^5$ M^{-2}.

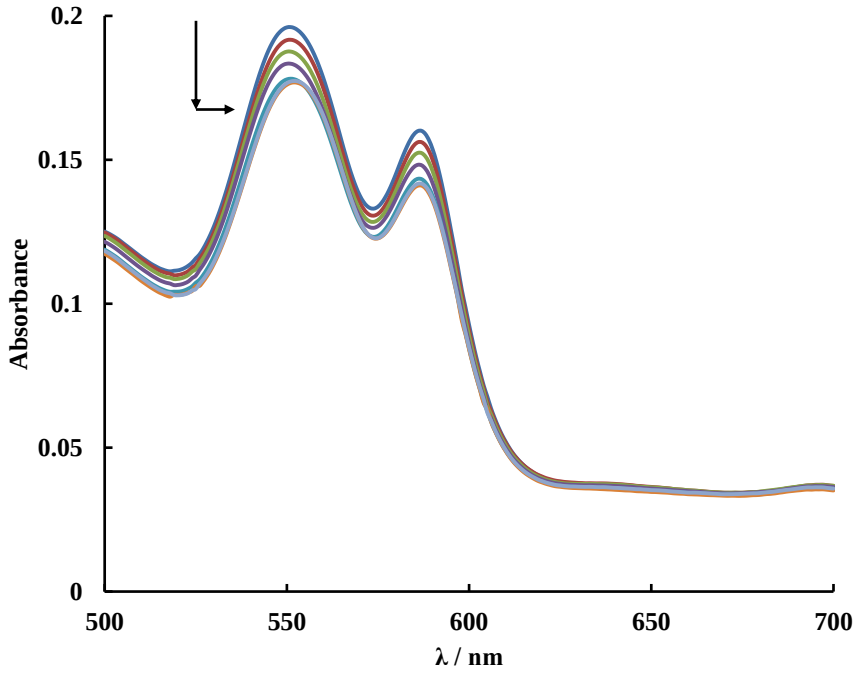

Fig. S11 Absorption spectral changes of 20 μM MndMIm$_4$P@CB[10] in the presence of imidazole in 100 mM phosphate buffer (pH 7.4). Concentration of imidazole ranged from 0 to 140 μM.

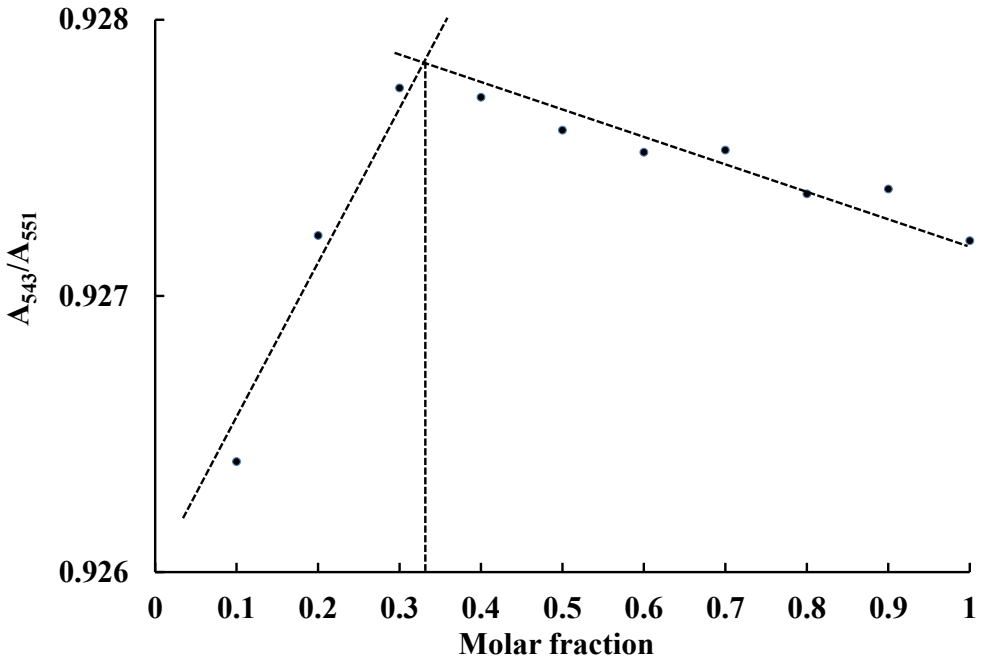

Fig. S12 Job`s plot analysis for mixture of MndMIm$_4$P@CB[10] and imidazole at a total concentration of 50 μM.

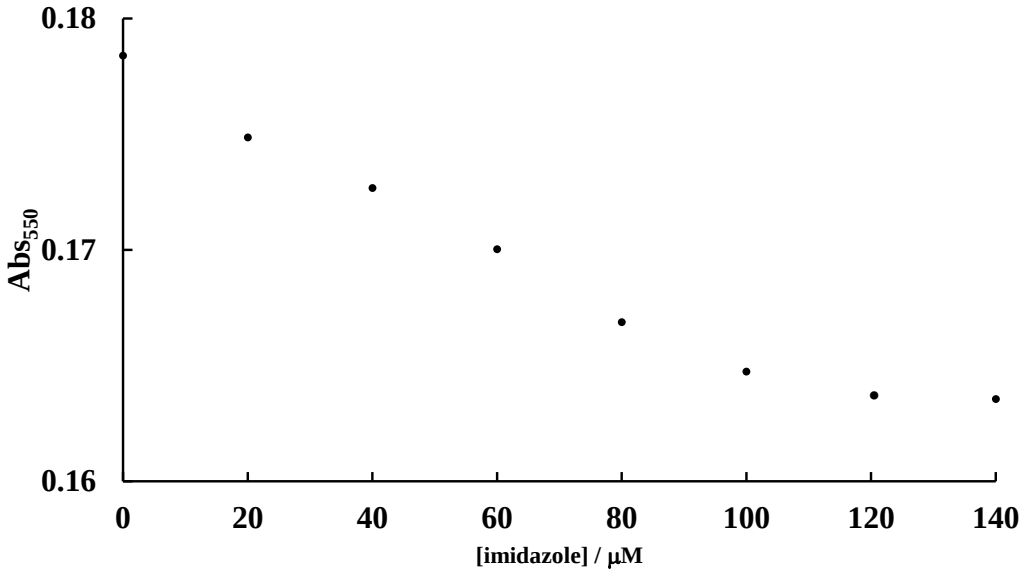

Fig. S13 Plot of absorbance at 550 nm of 20 μM MndMIm$_4$P@CB[10] as a function of imidazole concentration. The curve fitting analysis using TitrationFit program to determine $K_{a2} = 3.0\times10^8$ M^{-2}.

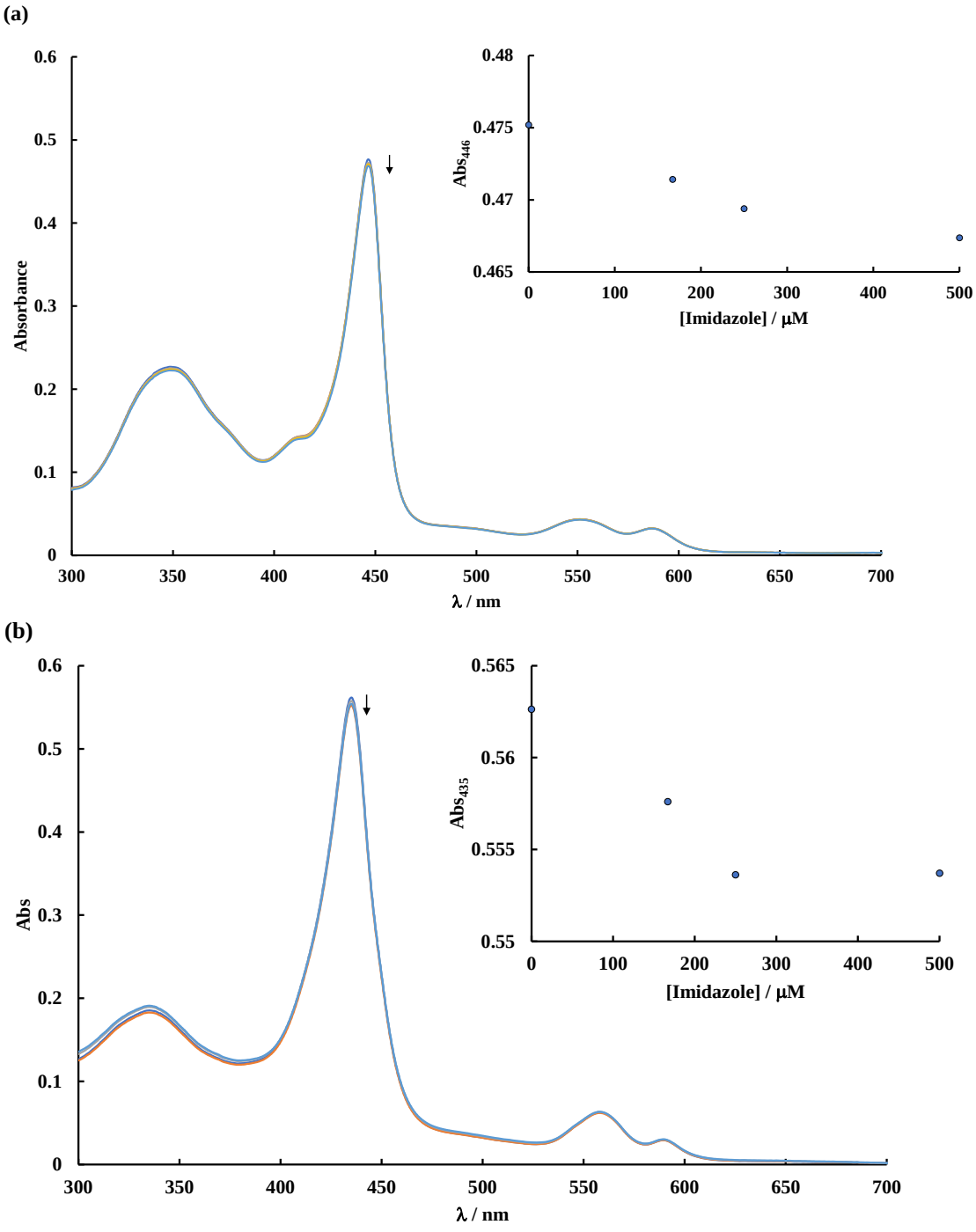

Fig. S14 Absorption spectral changes of MndMIm$_4$P@CB[10] in the presence of various concentrations of imidazole (0 ~ 500 μM). The spectral changes were monitored in water under acidic or basic conditions. (a) 100 mM acetate buffer (pH 4.5). (b) 100 mM phosphate buffer (pH 11). Insets show plots of absorbances of Soret bands as functions of imidazole concentration. The monitoring was performed at the lower MndMIm$_4$P@CB[10] concentration (3.5 μM) than 20 μM (Fig. S11 and S13) due to unexpected precipitation of MndMIm$_4$P@CB[10].

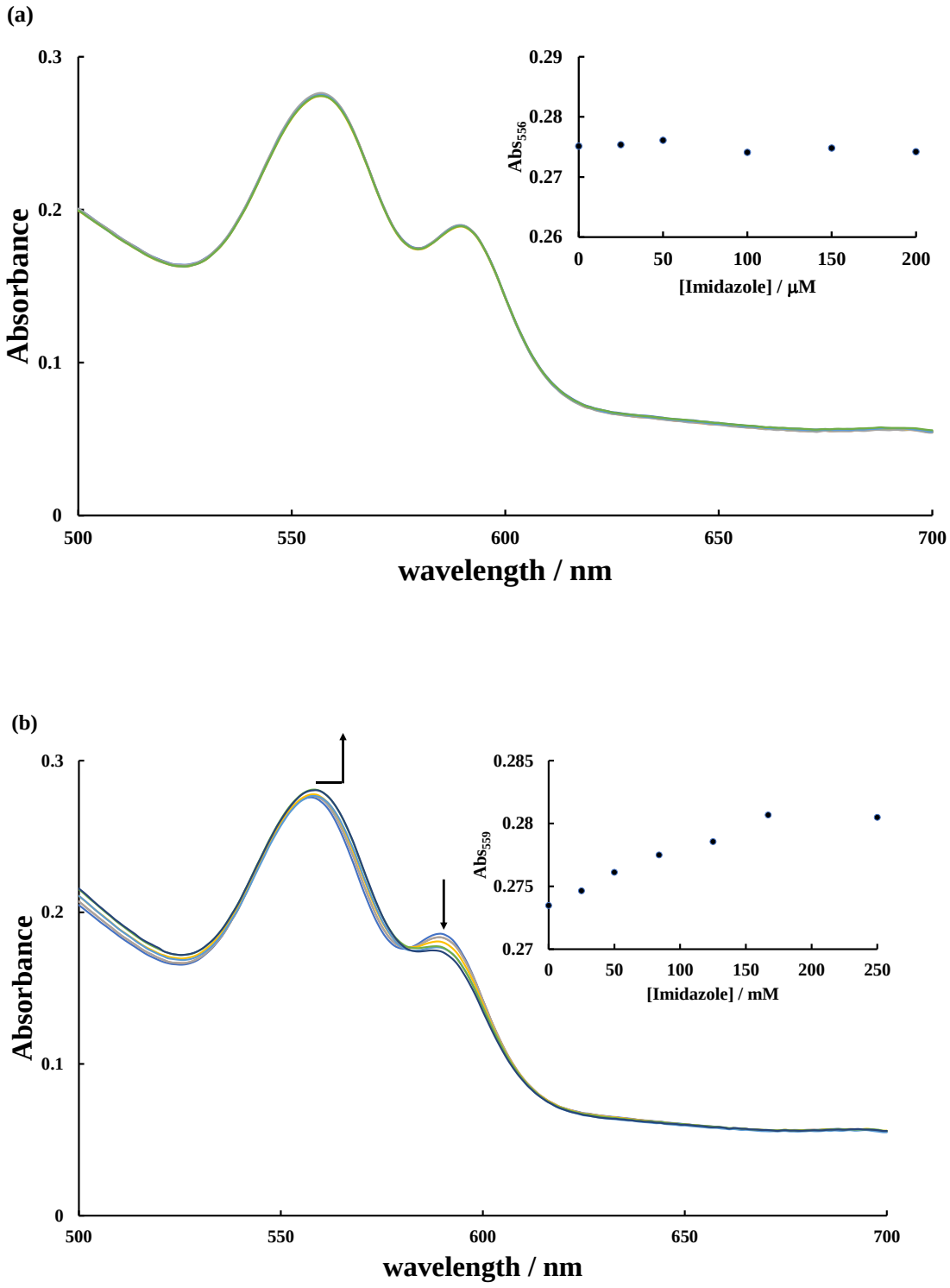

Fig. S15 Absorption spectral changes of 25 μM MndMIm$_4$P alone in 100 mM phosphate buffer (pH 7.4) in the presence of various concentrations of imidazole. (a) From 0 μM to 200 μM. (b) From 25 mM to 250 mM (large excess). Insets show plots of absorbance as functions of [Imidazole].

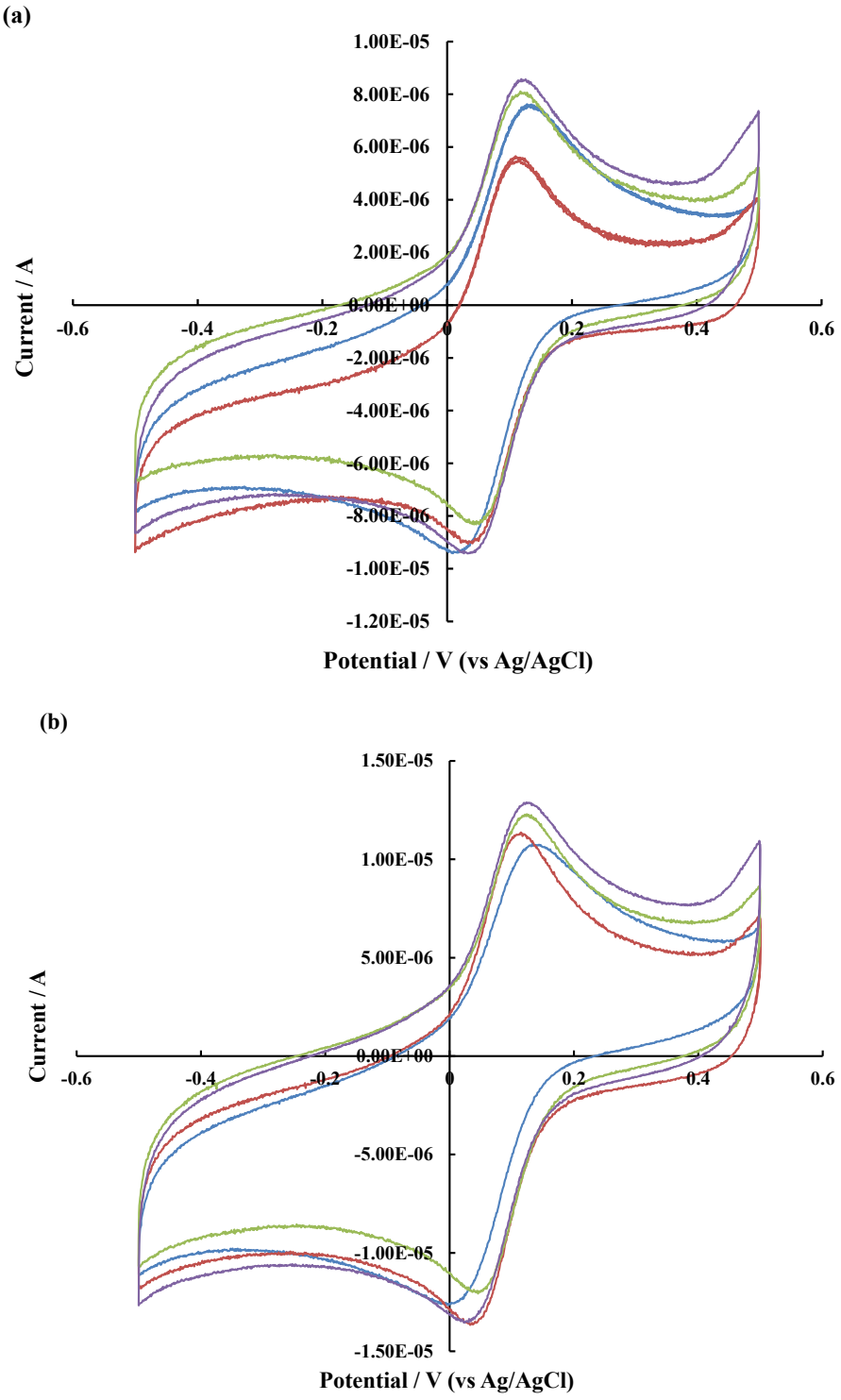

Fig. S16 Cyclic voltammogram of $MndMIm_4P$ alone (blue), $MndMIm_4P$@CB[10] (red), mixture of $MndMIm_4P$ and imidazole (six equivalents for $MndMIm_4P$) (purple), and $MndMIm_4P$@CB[10] (green). Supporting electrolyte: 10 mM phosphate buffer (pH 7.0) containing 50 mM Na_2SO_4. Scanning rate: (a) 50 mV/s, (b) 100 mV/s.

Table S1 Redox potential ($E_{1/2}$ for $Mn^{III/II}$ redox couple) versus normal hydrogen electrode (vs NHE).

	$E_{1/2}$ for $Mn^{III/II}$ (mV vs NHE)[a]
$MndMIm_4P$	**+ 280**
$MndMIm_4P$@CB[10]	**+ 270**
$MndMIm_4P$ + Im	**+ 280**
$MndMIm_4P$@CB[10];Im	**+ 280**

[a] $E_{1/2}$ values (vs Ag/AgCl) obtained from Fig. S16 were converted to those vs NHE by adding 200 mV. For stoichiometric formation of $MndMIm_4P$@CB[10];Im, $MndMIm_4P$@CB[10] was mixed with six equivalents of imidazole (Fig. S11~S13). The same molar ratio was traced for mixture of $MndMIm_4P$ and imidazole ($MndMIm_4P$ + Im).

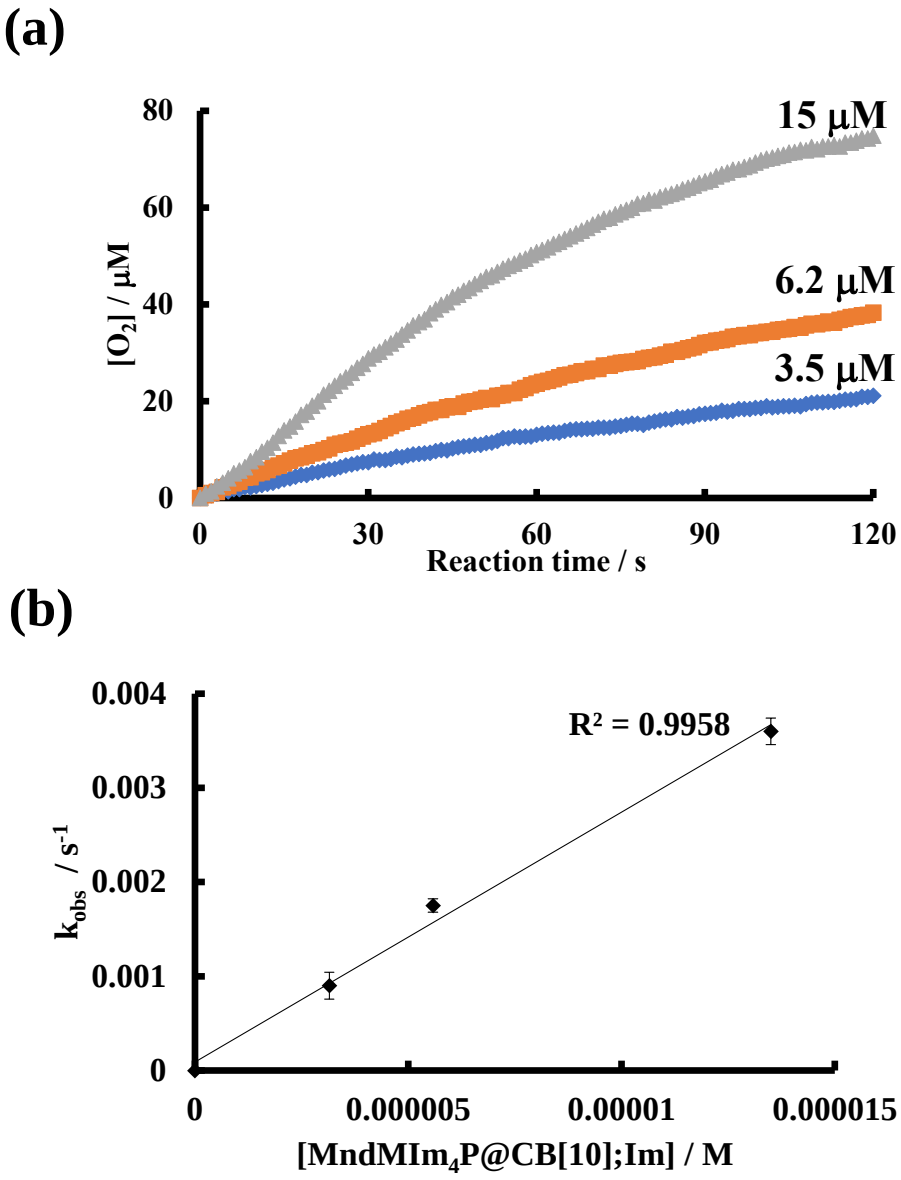

Fig. S17 (a):Time course of oxygen production from 1 mM H_2O_2 (final concentration) catalyzed by $MndMIm_4P$@CB[10];Im (six equivalents of imidazole to $MndMIm_4P$@CB[10]) in 100 mM phosphate buffer (pH 7.4) at 25℃. (b):Plot of observed rate constant (k_{obs}) as a function of the concentration of $MndMIm_4P$@CB[10];Im (per $MndMIm_4P$@CB[10]).

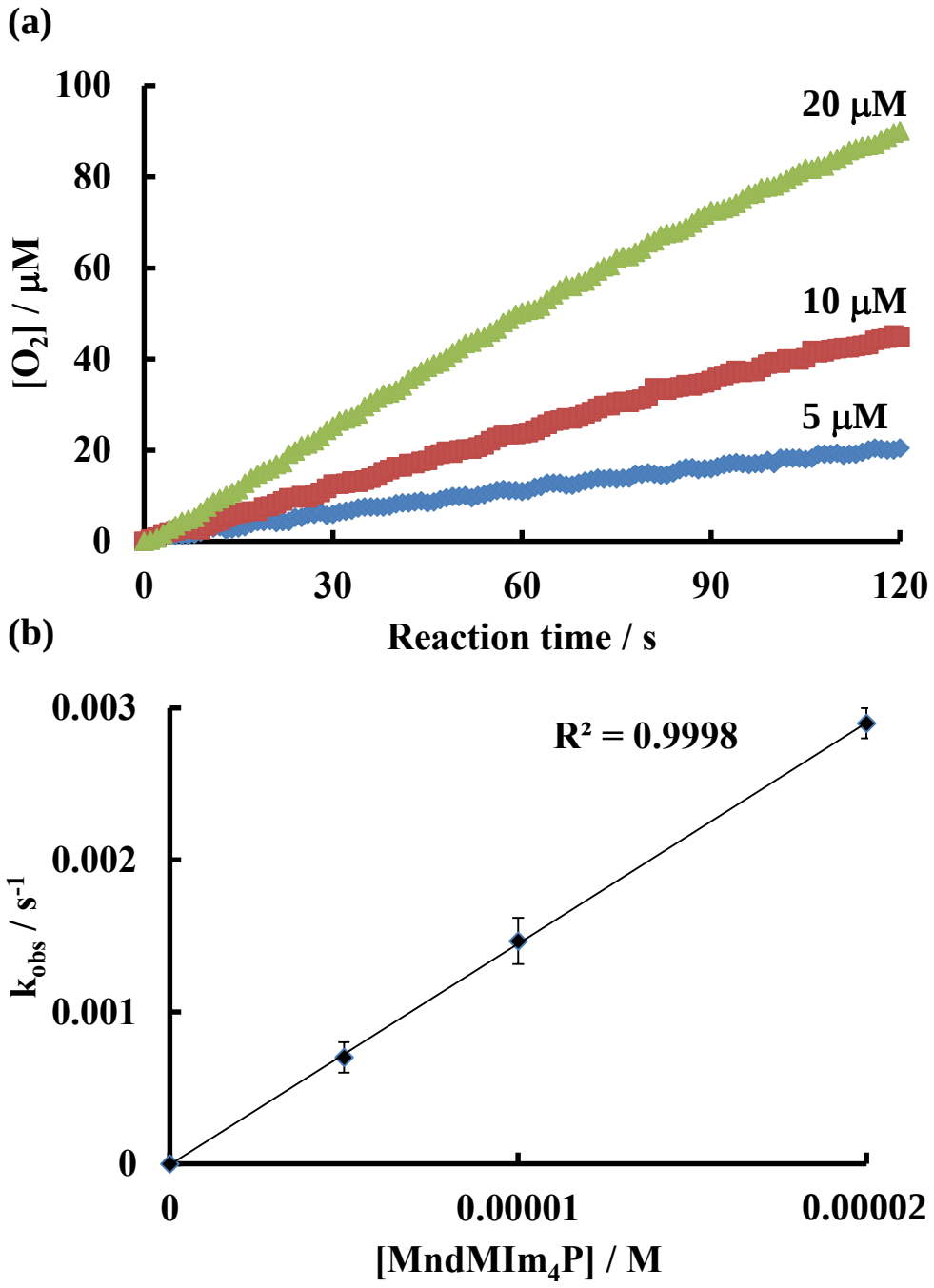

Fig. S18 (a) Time course of oxygen production from 1 mM H_2O_2 (final concentration) catalyzed by $MndMIm_4P$ in 100 mM phosphate buffer (pH 7.4) at 25℃. (b) Plot of observed rate constant (k_{obs}) as a function of the $MndMIm_4P$ concentration.

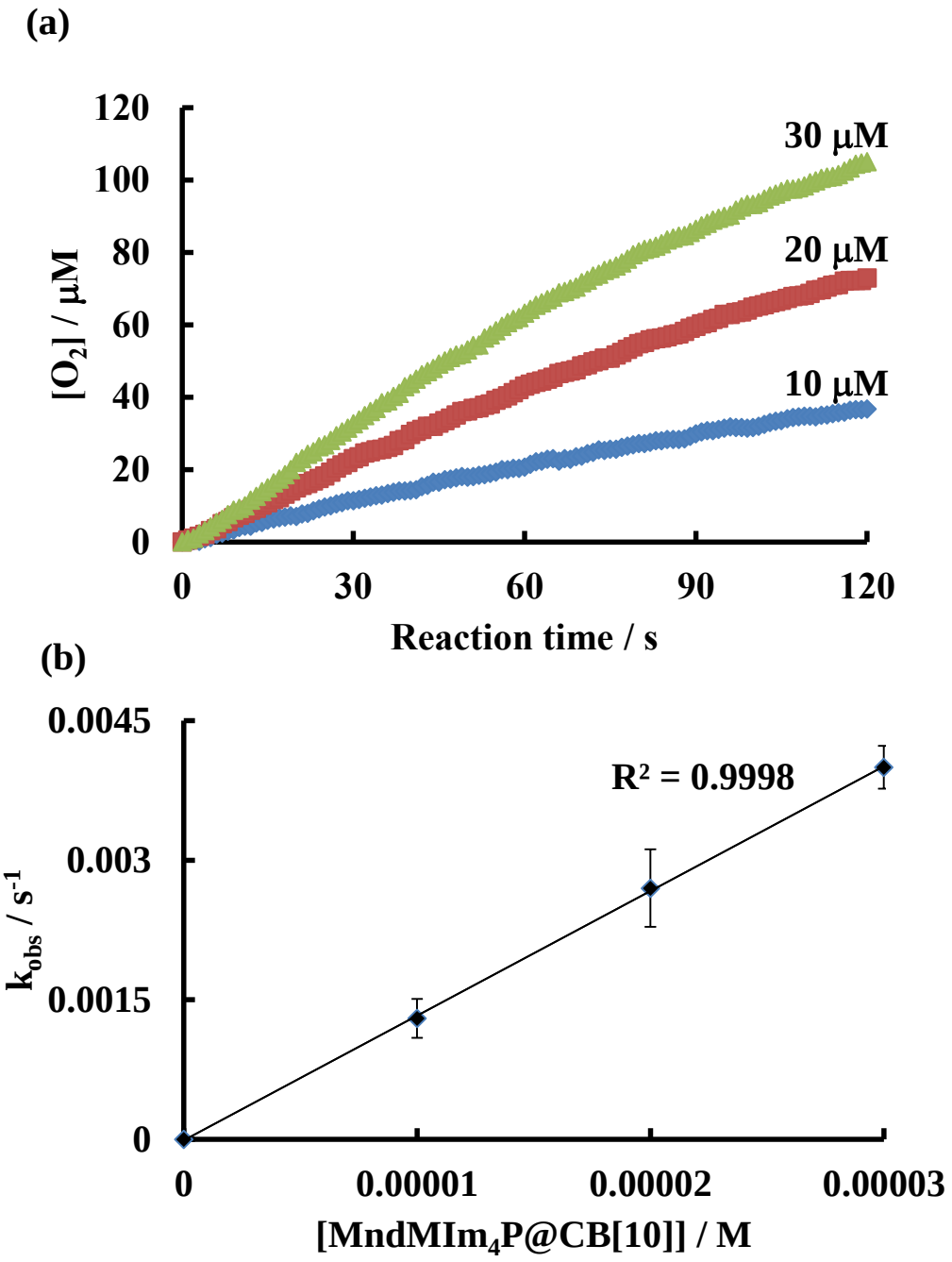

Fig. S19 (a) Time course of oxygen production from 1 mM H_2O_2 (final concentration) catalyzed by $MndMIm_4P@CB[10]$ in 100 mM phosphate buffer (pH 7.4) at 25℃. (b) Plot of observed rate constant (k_{obs}) as a function of the $MndMIm_4P@CB[10]$ concentration.

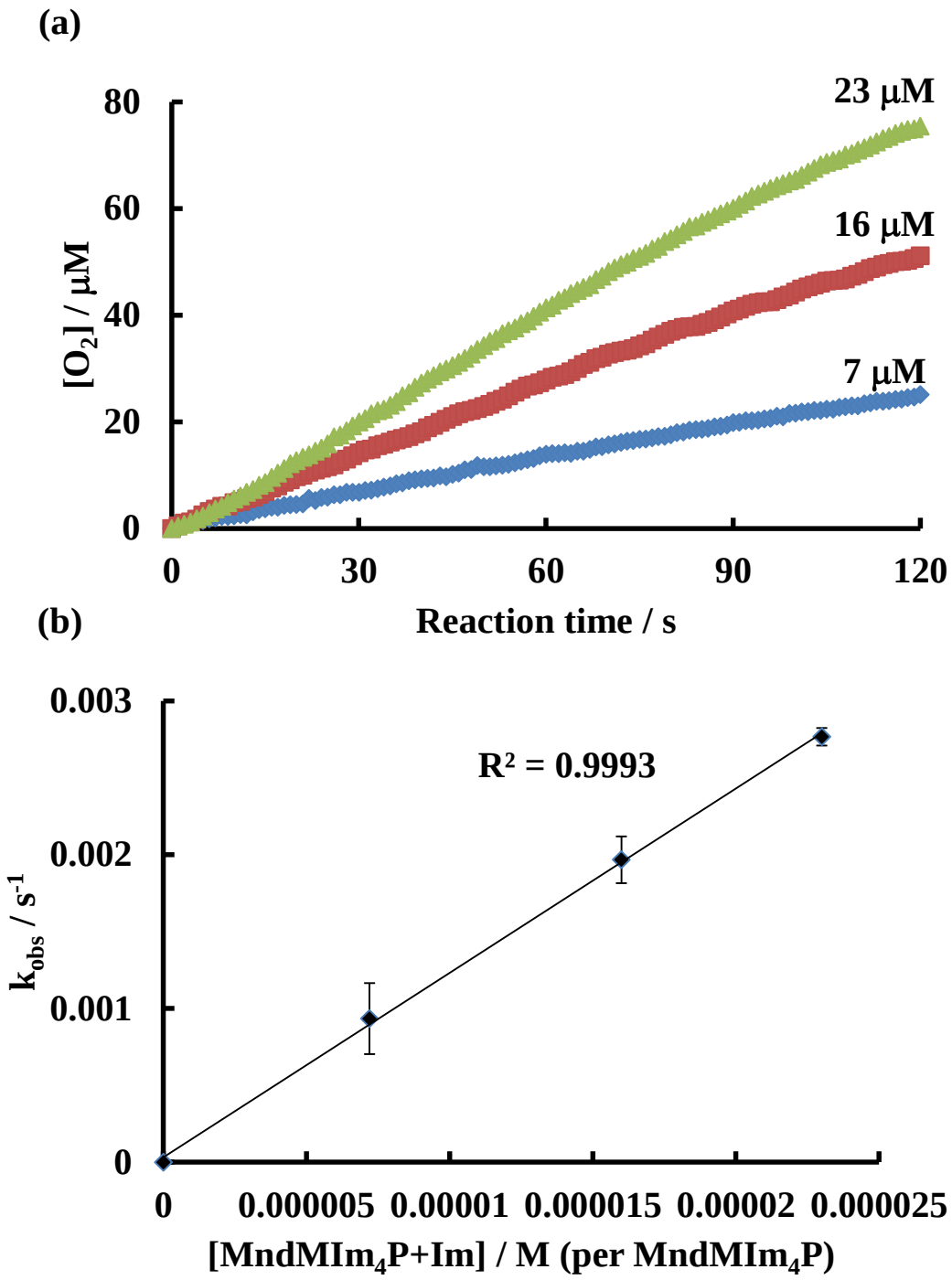

Fig. S20 (a) Time course of oxygen production from 1 mM H_2O_2 (final concentration) catalyzed by $MndMIm_4P$ in the presence of six equivalents of imidazole (Im) in 100 mM phosphate buffer (pH 7.4) at 25℃. (b) Plot of observed rate constant (k_{obs}) as a function of the $MndMIm_4P$+ Im concentration (per $MndMIm_4P$).

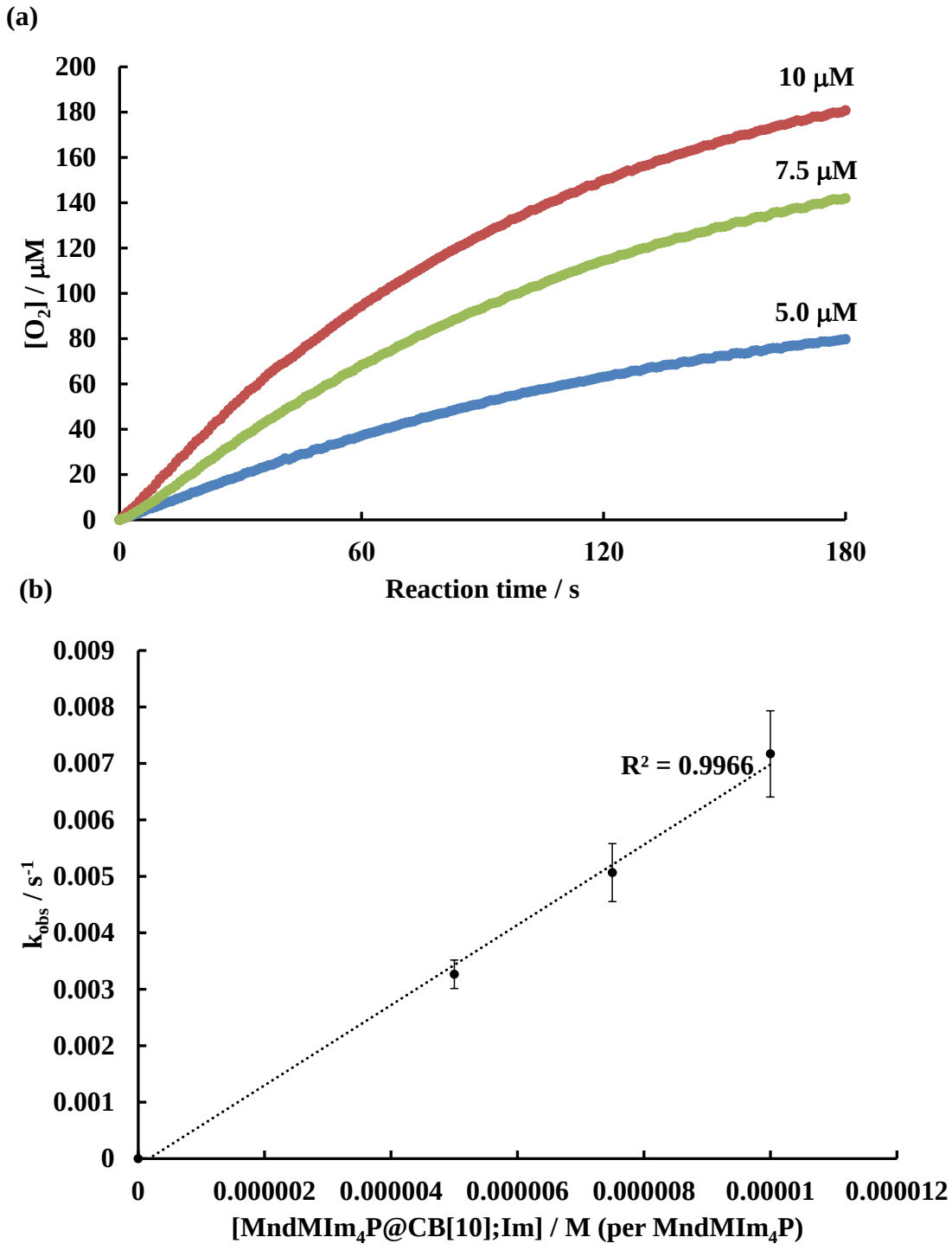

Fig. S21 (a) Time course of O_2 production from 10 mM H_2O_2 (final concentration) catalyzed by $MndMIm_4P$@CB[10];Im (six equivalents of imidazole to $MndMIm_4P$@CB[10]) in 50 mM phosphate buffer (pH 7.4) at 25℃. Yellow: 5.0 μM. Red: 7.5 μM. Green: 10 μM. (b) Plot of observed rate constant (k_{obs}) as a function of $MndMIm_4P$@CB[10];Im concentration (per $MndMIm_4P$).

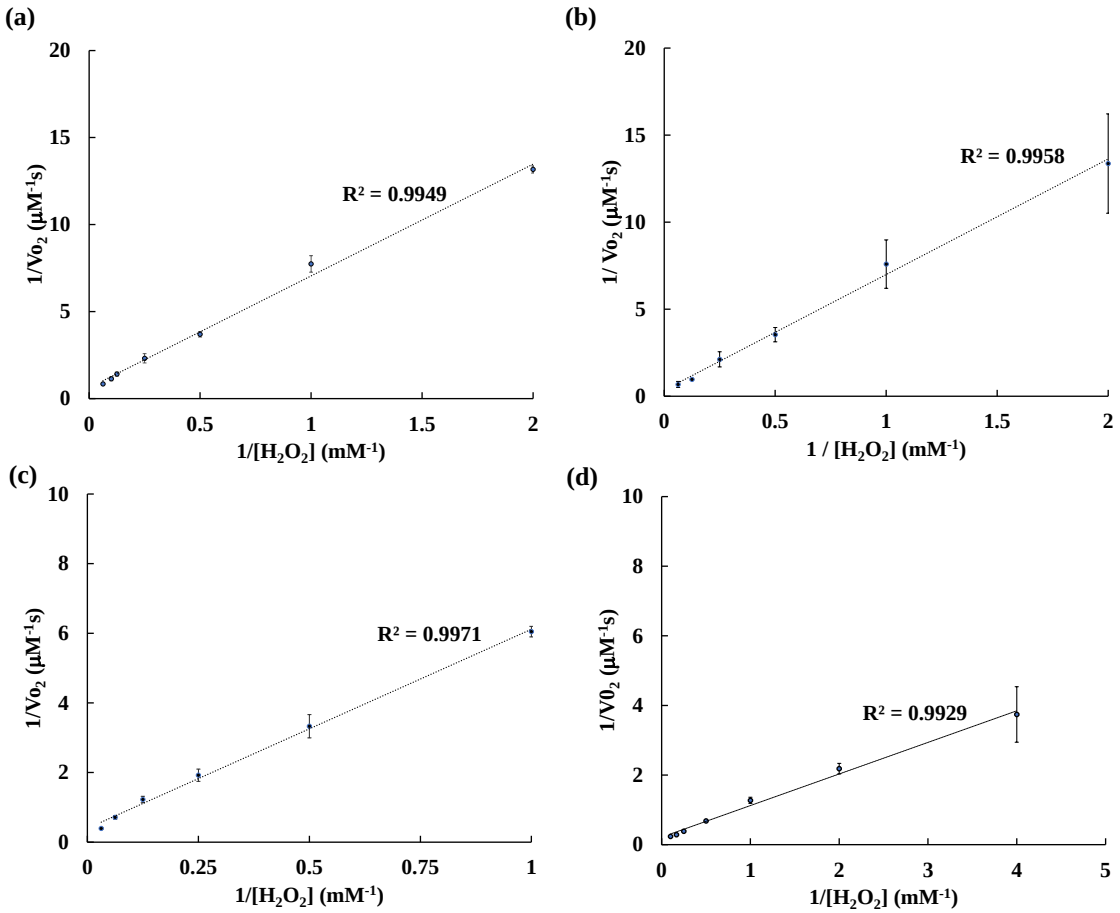

Fig. S22 Lineweaver-Burk plot for (a) MndMIm$_4$P alone, (b) MndMIm$_4$P@CB[10], (c) MndMIm$_4$P + Im and (d) MndMIm$_4$P@CB[10];Im. Turnover number (k_{cat}) and Michaelis constant (K_M) were determined by intercepts of the Lineweaver-Burk plot ($1/Vo_2$ axis for k_{cat} and $1/[H_2O_2]$ axis for K_M, respectively). The k_{cat} and K_M values were determined as averages for independent three runs.

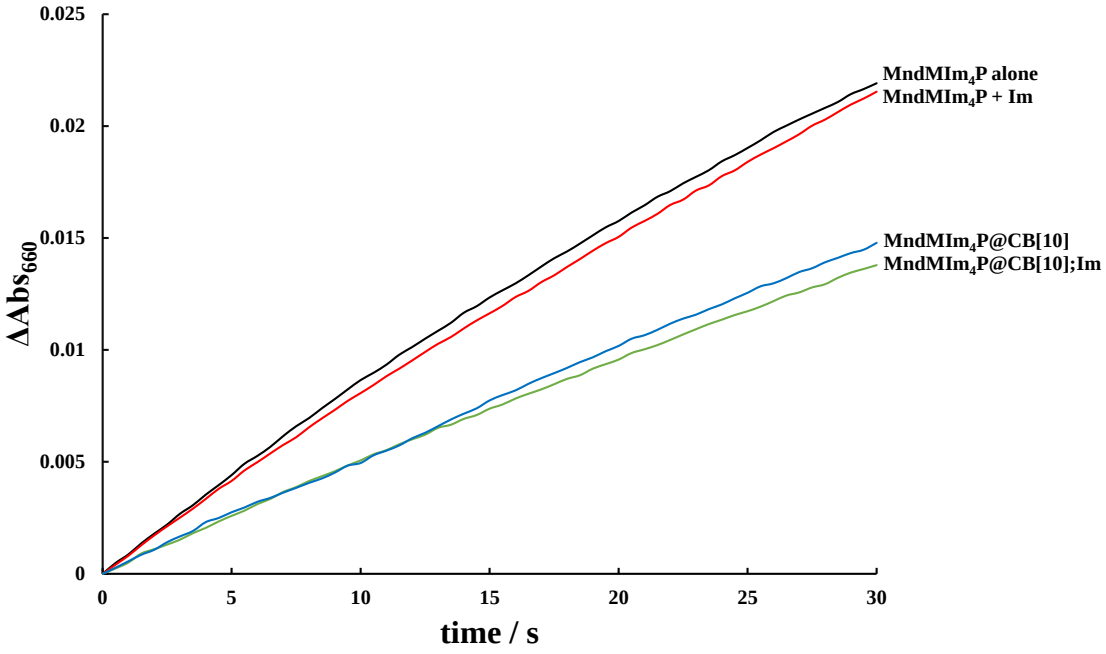

Fig. S23 Time course of absorbance at 660 nm (oxidized ABTS) in the presence of 0.2 mM H_2O_2 (final concentration), 0.5 mM ABTS (final concentration) and 15 μM (final concentration) test samples in 50 mM phosphate buffer (pH 7.4) at 25℃.

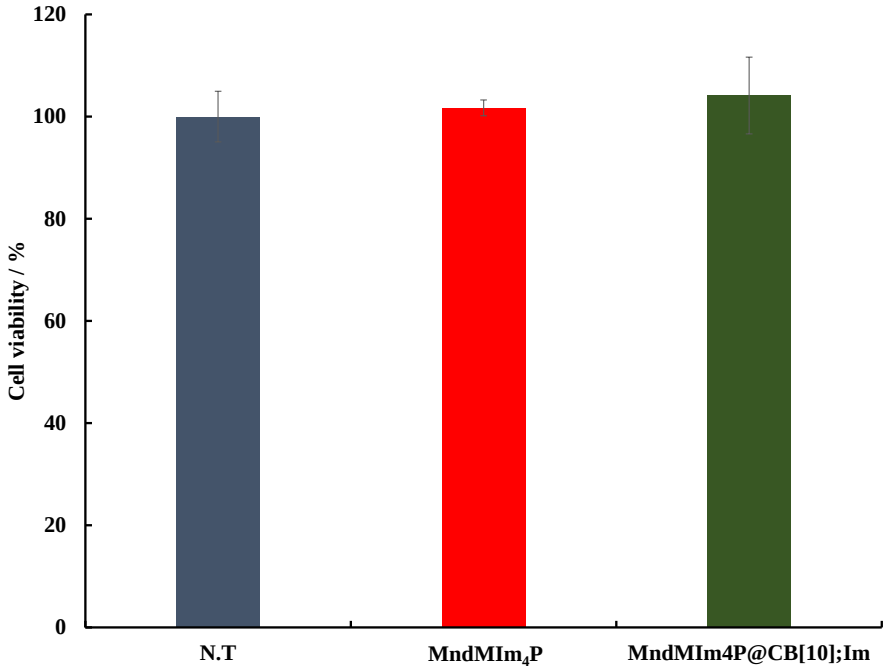

Fig. S24 Effect of 10 μM (final concentration) $MndMIm_4P$ or $MndMIm_4P$@CB[10];Im (per $MndMIm_4P$@CB[10]) on viability of HeLa cells. The cell viability was measured by Alamar blue assay. N.T: Non-treatment. No significant difference was observed in the cell viability among the three lanes.

Table S2 Literature benchmarks for catalase activity and peroxidase activity of Mn-Salen derivatives.

	Catalase activity (μM O_2/min)	Peroxidase activity (μM ABTS/min)	Reference
Mn-Salen derivative with distal imidazole	**83**[a]	**6.5**[c]	**1**
Mn-Salen derivative with distal pyridine	**281**[a]	**17.9**[c]	**1**
EUK-114	**70 ± 8**[b]	**0.8 ± 0.2**[d]	**2**
EUK-134	**243 ± 18**[b]	**37.8 ± 9.6**[d]	**2**
EUK-123	**112 ± 14**[b]	**19.9 ± 0.5**[d]	**2**

[a]Catalase activity was measured in 50 mM phosphate buffer (pH 7.4) by Clark-type oxygen electrode.[1] Oxygen production from 10 mM H_2O_2 (final concentration) catalyzed by 10 μM Mn-Salen derivatives was monitored at 25±0.2℃.[1] [b]Catalase activity was measured in sodium phosphate buffer (pH 8.1) by Clark-type oxygen electrode.[2] Oxygen production from 10 mM H_2O_2 (final concentration) catalyzed by 10 μM Mn-Salen derivatives was monitored at 27±0.2℃.[2] [c]Peroxidase activity was measured in the mixture consisted of 50 mM sodium phosphate (pH 7.4), 0.5 mM ABTS, 0.2 mM H_2O_2 and 10 μM Mn-Salen derivatives at 25±0.2℃.[1] [d]Peroxidase activity was measured in the mixture consisted of 50 mM sodium phosphate (pH 8.1), 0.9% sodium chloride, 0.5 mM ABTS, 0.2 mM H_2O_2 and 10 μM Mn-Salen derivatives (EUK-114, EUK-134, EUK-123) at 27±0.2℃.[2]

Table S3 SOD activity (k_{SOD}) and $ONOO^-$-reducing activity (k_{red}).

	SOD activity (k_{SOD}) ($\times 10^7$ $M^{-1}s^{-1}$)[a]	**$ONOO^-$-reducing activity (k_{red}) ($\times 10^6$ $M^{-1}s^{-1}$)[b]**	**Reference**
Mn-SOD (human)	**~ 200**	–	**3**
Peroxiredoxin Glutathione peroxidase	–	**8 ~ 70**	**4**
$MndMIm_4P$	**4.3 ± 0.3**	**4.2 ± 0.4**	**this work**
$MndMIm_4P$@CB[10]	**5.3 ± 0.7**	**5.5 ± 0.5**	**this work**
$MndMIm_4P$ + Im	**3.6 ± 1.1**	**5.2 ± 0.2**	**this work**
$MndMIm_4P$@CB[10];Im	**5.0 ± 0.5**	**7.6 ± 0.8**	**this work**
$MnM4Py_4P$	**2.1 ± 0.1**	**2.0 ± 0.2**	**this work**

[a]SOD activity was determined by Stopped-flow method according to the previous procedure.[5-7] Briefly, time decay of superoxide at 245 nm was spectrophotometrically monitored in HEPES buffer (pH 8.1) at 21℃.[7] For each concentration of sample, observed rate constant (k_{obs}) was calculated. k_{SOD} was determined from the slope of the plot of k_{obs} as a function of the sample concentration. SOD activity of Mn(III)-5,10,15,20-tetrakis(*N*-methylpyridinium-4-yl)porphyrin ($MnM4Py_4P$) (control experiment) is consistent with that of the previous report.[7] [b]$ONOO^-$-reducing activity was determined by the similar procedure to that for SOD activity.[5-8] Time decay of $ONOO^-$at 302 nm was spectrophotometrically monitored in the presence of 2 mM ascorbic acid (Asc) in 50 mM phosphate buffer (pH 7.4) at 25℃. The subsequent protocol is same as that for SOD activity. The catalytic rate constant (k_{red}) of ca. ~10^6 $M^{-1}s^{-1}$ for $MnM4Py_4P$ was obtained as previously reported.[5,8]
[a,b]For stoichiometric formation of $MndMIm_4P$@CB[10];Im, $MndMIm_4P$@CB[10] was mixed with six equivalents of imidazole to $MndMIm_4P$@CB[10] (Fig. S11~S13). The same molar ratio was traced for mixture of $MndMIm_4P$ and imidazole ($MndMIm_4P$ + Im).

References

1. Y. Noritake, N. Umezawa, N. Kato, T. Higuchi, *Inorg. Chem*., 2013, **52**, 3653－3662.
2. S. R. Doctrow, K. Huffman, C. B. Marcus, G. Tocco, E. Malfroy, C. A. Adinolfi, H. Kruk, K. Baker, N. Lazarowych, J. Mascarenhas, B. Malfroy, *J. Med. Chem*., 2002, **45**, 4549－4558.
3. A. Squarcina, A. Soraru, F. Rigodanza, M. Carraro, G. Brancatelli, T. Carofiglio, S. Geremia, V. Larosa, T. Morosinotto, M. Bonchio, *ACS Catal*., 2017, **7**, 1971－1976.
4. A. Haber, Z. Gross, *Chem. Commun*., 2015, **51**, 5812－5827.
5. S. Asayama, T. Nakajima, H. Kawakami, *Metallomics*, 2011, **3**, 744－748.
6. R. Kubota, S. Imamura, T. Shimizu, S. Asayama, H. Kawakami, *ACS Med. Chem. Lett*., 2014, **5**, 639－643.
7. F. C. Friedel, D. Lieb, I. Ivanovic-Burmazovic, *J. Inorg. Biochem*., 2012, **109**, 26－32.
8. J. Lee, J. A. Hunt, J. T. Groves, *J. Am. Chem. Soc*., 1998, **120**, 6053－6061.